Neurobiology of Disease

Stimulated Emission Depletion (STED) Microscopy Reveals Nanoscale Defects in the Developmental Trajectory of Dendritic Spine Morphogenesis in a Mouse Model of Fragile X Syndrome

Lasani S. Wijetunge,[1,2,3] Julie Angibaud,[2,3] Andreas Frick,[4,5] Peter C. Kind,[1,6]* and U. Valentin Nägerl[2,3]*

[1]Patrick Wild Centre, University of Edinburgh, Edinburgh EH8 9XD, United Kingdom, [2]Interdisciplinary Institute for Neuroscience, Université de Bordeaux, Bordeaux 33077, France, [3]Interdisciplinary Institute for Neuroscience, Centre National de la Recherche Scientifique UMR 5297, Bordeaux 33077, France, [4]Institut National de la Santé et de la Recherche Médicale, [5]Université de Bordeaux, Neurocentre Magendie, Physiopathologie de la Plasticité Neuronale, U862, Bordeaux 33077, France, and [6]Centre for Brain Development and Repair, inStem, Bangalore, India

Dendritic spines are basic units of neuronal information processing and their structure is closely reflected in their function. Defects in synaptic development are common in neurodevelopmental disorders, making detailed knowledge of age-dependent changes in spine morphology essential for understanding disease mechanisms. However, little is known about the functionally important fine-morphological structures, such as spine necks, due to the limited spatial resolution of conventional light microscopy. Using stimulated emission depletion microscopy (STED), we examined spine morphology at the nanoscale during normal development in mice, and tested the hypothesis that it is impaired in a mouse model of fragile X syndrome (FXS). In contrast to common belief, we find that, in normal development, spine heads become smaller, while their necks become wider and shorter, indicating that synapse compartmentalization decreases substantially with age. In the mouse model of FXS, this developmental trajectory is largely intact, with only subtle differences that are dependent on age and brain region. Together, our findings challenge current dogmas of both normal spine development as well as spine dysgenesis in FXS, highlighting the importance of super-resolution imaging approaches for elucidating structure–function relationships of dendritic spines.

Key words: **dendritic spines; development; fragile X syndrome; spine dysgenesis; STED; super-resolution microscopy**

Introduction

Spines are small protrusions of the postsynaptic membrane of dendrites that mediate most excitatory synaptic transmission in the cerebral cortex. Their density and morphology are closely linked to synaptic function (Yuste, 2011). Spine morphology thus has been used as a proxy for synaptic efficacy. Altered spine morphology is a hallmark of many neurodevelopmental disorders (NDDs), such as intellectual disability and autism spectrum disorder, which are commonly referred to as "synaptopathies" (Li et al., 2003; Brose et al., 2010; Penzes et al., 2011).

An understanding of spine dysgenesis associated with NDDs requires a detailed description of normal spine development. In the neocortex and hippocampus, the preeminent model of spine development states that spines develop from immature prototypic spines, called "filopodia," with a long and thin morphology, into more mature "mushroom" spines featuring large heads and narrow necks (for review, see Yuste and Bonhoeffer, 2004).

Fragile X syndrome (FXS), an archetypal example of an NDD, is traditionally associated with an increase in long and thin spines, suggesting a delay in synapse maturation. However, recent studies often fail to replicate this reported phenotype (for review, see He and Portera-Cailliau, 2013). To date, studies examining spine dysgenesis in FXS as well as normal spine development, have used diffraction-limited microscopy techniques, such as confocal and two-photon microscopy, which at best have a spatial resolution of 250 and 400 nm in brain slices, respectively. However, several parameters of spine morphology, such as head width, neck

Received Dec. 19, 2013; revised March 15, 2014; accepted April 1, 2014.

Author contributions: L.S.W., P.C.K., and U.V.N. designed research; L.S.W. and J.A. performed research; A.F. contributed unpublished reagents/analytic tools; L.S.W. analyzed data; L.S.W., J.A., A.F., P.C.K., and U.V.N. wrote the paper.

This work was supported by an international exchange grant from the Royal Society (P.C.K., U.V.N., L.S.W.), by proof-of-concept Eurobioimaging studies (L.S.W., U.V.N.), by the Medical Research Council (P.C.K.), by the Shirley Foundation (P.C.K., L.S.W.), by the Patrick Wild Centre (P.C.K., L.S.W.), by the Institut National de la Santé et de la Recherche Médicale (A.F.), by the Agence Nationale pour la Recherche (Programme Chaires d'Excellence grant to U.V.N.), by Human Frontier Science Program (U.V.N.) and by France-BioImaging (ANR-10-INSB-04, U.V.N.). The microscopy was performed at Bordeaux Imaging Center (BIC) of the Université de Bordeaux. We thank Philippe Legros (BIC) for technical support, and Jan Tonnesen (Université de Bordeaux), Tim O'Leary (Brandeis University), and Aleks Domanski (University of Edinburgh) for helpful discussions.

The authors declare no competing financial interests.

*P.C.K and U.V.N. contributed equally to this work.

Correspondence should be addressed to any of the following: Peter C. Kind, Patrick Wild Centre, University of Edinburgh, Edinburgh EH8 9XD, UK. E-mail: p.kind@ed.ac.uk; U. Valentin Nägerl, Interdisciplinary Institute for Neuroscience, CNRS UMR 5297, Bordeaux 33077, France. E-mail: valentin.nagerl@u-bordeaux.fr; or Lasani S. Wijetunge, University of Edinburgh, Edinburgh EH8 9XD, UK. E-mail: l.s.wijetunge@ed.ac.uk.

DOI:10.1523/JNEUROSCI.5302-13.2014

 0270-6474/14/336405-08$15.00/0

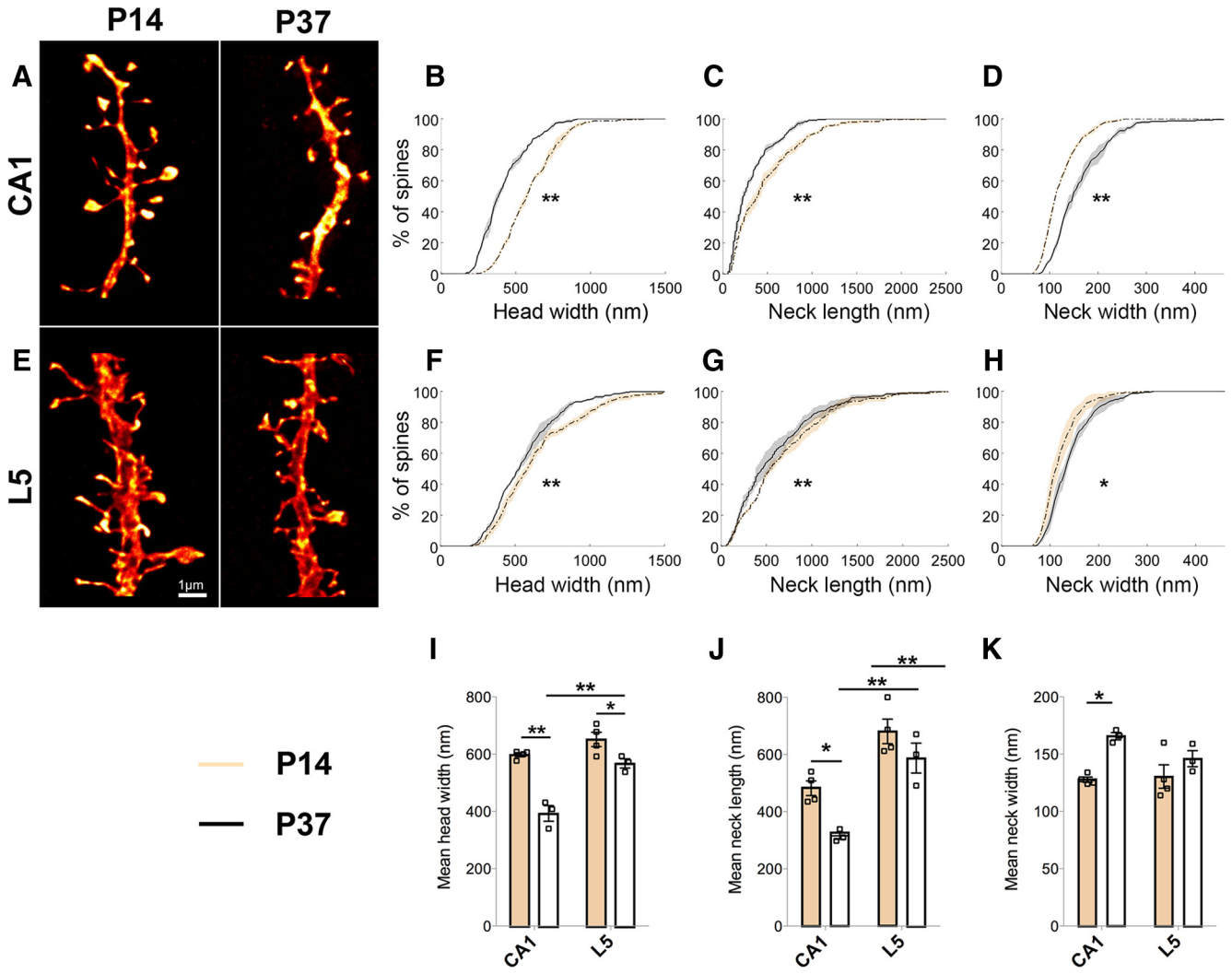

Figure 1. During development, spine heads become smaller and spine necks become shorter and wider. ***A***, ***E***, Dendritic segments from CA1 (***A***) and L5 pyramidal cells (***E***) examined at P14 and P37. ***B–D***, ***F–H***, Kolmogorov–Smirnov tests of the cumulative frequency distributions show that for both CA1 (***B–D***) and L5 pyramidal cells (***F–H***), the distribution profiles of spine head widths ($p < 0.001$ for CA1; $p < 0.02$ for L5), neck lengths ($p < 0.01$) and neck widths ($p < 0.001$) significantly differ between the two ages. Here, whether the *P* value is considered significant or not is corrected for using the false discovery rate method, which controls false positives during multiple comparisons. Using two-way ANOVA with *post hoc* Bonferroni multiple comparisons, mean differences in these parameters also show age and brain region-specific differences in the magnitude of the effects. ***I***, For head width, age effect: $F_{(1,10)} = 49.94$, $p < 0.0001$; region effect: $F_{(1,10)} = 31.16$, $p = 0.0002$; age × region interaction: $F_{(1,10)} = 8.79$, $p = 0.01$. ***J***, For neck length, age effect: $F_{(1,10)} = 12.25$, $p = 0.006$; region effect: $F_{(1,10)} = 40.14$, $p < 0.0001$. ***K***, For neck width, age-specific effect ($F_{(1,10)} = 14.61$, $p = 0.003$) only in CA1 ($p \leq 0.01$). Shaded areas around lines show interanimal variability. In bar graphs, data are represented as mean ± SEM, where n = number of animals. Scale bar, 1 μm. *$p < 0.05$; **$p < 0.01$.

length, and neck width, which are crucial determinants of synapse function, are often smaller than the resolution of these techniques (Harris et al., 1992).

Stimulated emission depletion (STED) microscopy overcomes this problem because it provides a much higher spatial resolution (~50 nm), permitting accurate and reliable measurements of these key morphological parameters (Hell and Wichmann, 1994; Nägerl et al., 2008; Bethge et al., 2013).

Using STED microscopy, we examined the developmental trajectory of spine morphogenesis in normal mice and tested the hypothesis that it is altered in a mouse model of FXS (*Fmr1*KO; Mientjes et al., 2006). To this end, we quantified the morphological parameters of dendritic spines at postnatal day (P) 14 and P37, which is the period in brain development when spine turnover decreases and synaptic circuits become fully established (Holtmaat et al., 2005).

Contrary to previous findings, we observed that spine heads become smaller and spine necks shorter and wider over this important developmental period. The aggregate effect of these morphological changes is consistent with a substantial increase in electrochemical coupling between spine and dendritic shaft. Surprisingly, the developmental trajectory of spine morphogenesis in *Fmr1*KO mice largely recapitulates that of wildtype mice, except for age-dependent and brain region-dependent alterations, which are only detectable at the nanoscale.

Materials and Methods

Transgenic animals. All experiments were performed in accordance with the European directive on the protection of animals used for scientific purposes (2010/63/EU).

All experiments were performed using the second-generation *Fmr1*KO mouse model (Mientjes et al., 2006). Double transgenic mice were obtained from cross breeding *Fmr1* heterozygous ($Fmr1^{+/-}$) female with Thy1-YFP-H homozygous (Thy-1YFP-H$^{-/-}$; Feng et al., 2000) male mice. The resulting progeny express yellow fluorescent protein (YFP) in a subpopulation of principal neurons in the hippocampus as well as in layer (L) 5 of cortex (Feng et al., 2000; Porrero et al., 2010; all

Table 1. Summary of spine morphological parameters

	P14		P37	
Morphology parameter	Wildtype	*Fmr1*KO	Wildtype	*Fmr1*KO
CA1				
Head width				
Range	244–1367 nm	152–1534 nm	165–918 nm	175–1122 nm
Mean ± SD per animal	598 ± 15 nm	586 ± 49 nm	393 ± 47 nm	447 ± 21 nm
95% CI on mean	584–612 nm	543–629 nm	340–446 nm	423–471 nm
Median ± SD per animal	577 ± 28 nm	556 ± 63 nm	360 ± 45 nm	415 ± 28 nm
Neck length				
Range	81–2307 nm	61–2080 nm	61–1164 nm	62–1064 nm
Mean ± SD per animal	482 ± 51 nm	481 ± 52 nm	316 ± 21 nm	264 ± 45 nm
95% CI on mean	432–532 nm	435–527 nm	292–340 nm	212–315 nm
Median ± SD per animal	416 ± 72 nm	376 ± 53 nm	239 ± 24 nm	211 ± 24 nm
Neck width				
Range	66–258 nm	60–265 nm	84–465 nm	81–353 nm
Mean ± SD per animal	128 ± 4 nm	132 ± 13 nm	165 ± 6 nm	150 ± 4 nm
95% CI on mean	124–132 nm	121–144 nm	159–172 nm	144–158 nm
Median ± SD per animal	118 ± 2 nm	124 ± 15 nm	151 ± 8 nm	141 ± 12 nm
L5				
Head width				
Range	217–1556 nm	142–1376 nm	201–1560 nm	185–1238 nm
Mean ± SD per animal	652 ± 51 nm	619 ± 39 nm	568 ± 28 nm	554 ± 39 nm
95% CI on mean	602–701 nm	588–650 nm	536–599 nm	510–598 nm
Median ± SD per animal	593 ± 53 nm	590 ± 25 nm	532 ± 41 nm	535 ± 34 nm
Neck length				
Range	62–2514 nm	81–3192 nm	61–2351 nm	82–2553 nm
Mean ± SD per animal	681 ± 86 nm	688 ± 89 nm	587 ± 91 nm	523 ± 61 nm
95% CI on mean	597–765 nm	617–760 nm	484–690 nm	454–592 nm
Median ± SD per animal	617 ± 80 nm	577 ± 143 nm	481 ± 124 nm	439 ± 78 nm
Neck width				
Range	67–300 nm	65–383 nm	70–318 nm	72–369 nm
Mean ± SD per animal	130 ± 21 nm	119 ± 12 nm	146 ± 12 nm	141 ± 20 nm
95% CI on mean	110–150 nm	110–129 nm	133–160 nm	119–164 nm
Median ± SD per animal	124 ± 20 nm	111 ± 10 nm	134 ± 8 nm	130 ± 21 nm

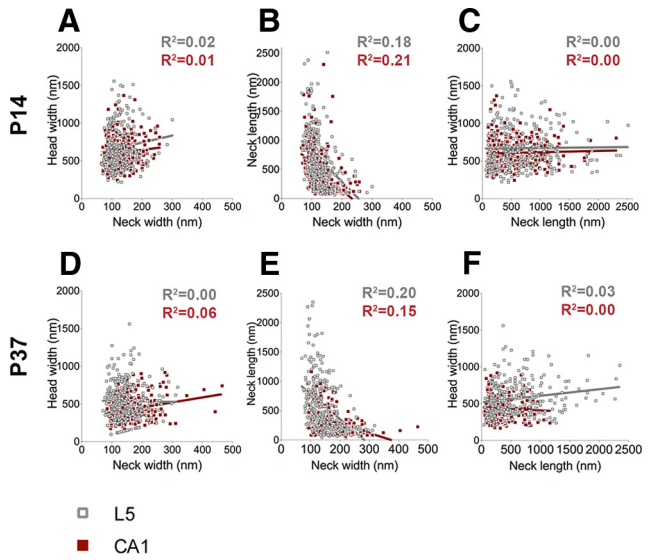

Figure 2. Absence of correlation between spine morphological parameters. ***A–F***, Spine morphological parameters do not appear to strongly covary with each other in CA1 or L5 at either P14 (***A–C***) or P37 (***D–F***). At P14, there are no correlations between spine head width and neck width (***A***: for CA1, $R^2 = 0.01$; for L5, $R^2 = 0.02$) or between spine head width and neck length (***C***: for CA1 and L5, $R^2 = 0.00$). Similarly, no correlations are observed between these parameters at P37 either (***D***: head width vs neck width for CA1, $R^2 = 0.06$; for L5, $R^2 = 0.00$; ***F***: head width vs neck length for CA1, $R^2 = 0.00$; for L5, $R^2 = 0.03$). A weak negative correlation is observed between spine neck length and neck width in both brain regions at both ages [***B***: at P14, for CA1, $R^2 = 0.21$ ($p < 0.001$); for L5, $R^2 = 0.18$ ($p < 0.001$); ***E***: at P37, for CA1, $R^2 = 0.15$ ($p < 0.001$); for L5, $R^2 = 0.20$ ($p < 0.001$)], suggesting that longer necks are likely to be narrower and vice versa. In scatter plots, the red symbols represent data from CA1 and gray symbols represent data from L5.

on a C57BL/6J background). Only male mice that were either $Fmr1^{+/y}$ (wildtype) or $Fmr1^{-/y}$ (*Fmr1*KO) with respect to the *Fmr1* allele were used for these experiments, and were killed at P14 and P37. Tissue preparation, imaging, and all analysis were all performed blind to genotype.

Tissue preparation and immunohistochemistry. Mice were killed with a lethal dose of sodium pentobarbital (200 mg/kg, i.p.; Centravet) and perfused transcardially with saline followed by 4% (w/v) paraformaldehyde in 0.1 M phosphate buffer, pH 7.4. Brains were removed, postfixed in 4% paraformaldehyde for 6–8 h, and then sectioned in the coronal plane on a vibratome at 40–50 μm. The endogenous expression of YFP signal was enhanced on selected brain sections containing the dorsal hippocampus and posterior medial barrel subfield as follows: free-floating sections blocked and permeabilized with a blocking buffer containing 5% normal goat serum and 0.5% TX-100; incubated with the rabbit anti-GFP (1:1000; Invitrogen) for 24 h; and visualized using the photostable Atto 647N-conjugated goat anti-rabbit secondary antibody (1:500; Sigma-Aldrich). The sections were mounted on coverslips using Mowiol.

STED microscopy. Images were obtained using a commercial STED microscope (Leica TCS SP5 STED, Leica Microsystems). The STED module (Leica Microsystems) used a pulsed diode laser to excite fluorescence at 635 nm and a TiSaphire-based pulsed laser for fluorescence quenching at 775 nm (Mai Tai, Spectra-Physics).

Image acquisition. Image stacks of well isolated apical dendritic segments of CA1 pyramidal cells within the stratum radiatum and apical oblique dendrites of L5 cells within upper L5 and the L4/5 boundary were imaged at an imaging depth of <15 μm. The image stacks were Nyquist sampled using an HCX Plan Apo CS STED X100 lens (numerical aperture, 1.4; oil immersion) and acquired with a pixel size of ~20 nm, a *z*-step size of 250 nm, and at a scan speed of 200 Hz using six line averages. All image stacks were deconvolved using the STED deconvolution module of Huygens 4.2 (Scientific Volume Imaging).

Image analysis. Measurements of spine morphological parameters were done using ImageJ (National Institutes of Health). Neck length

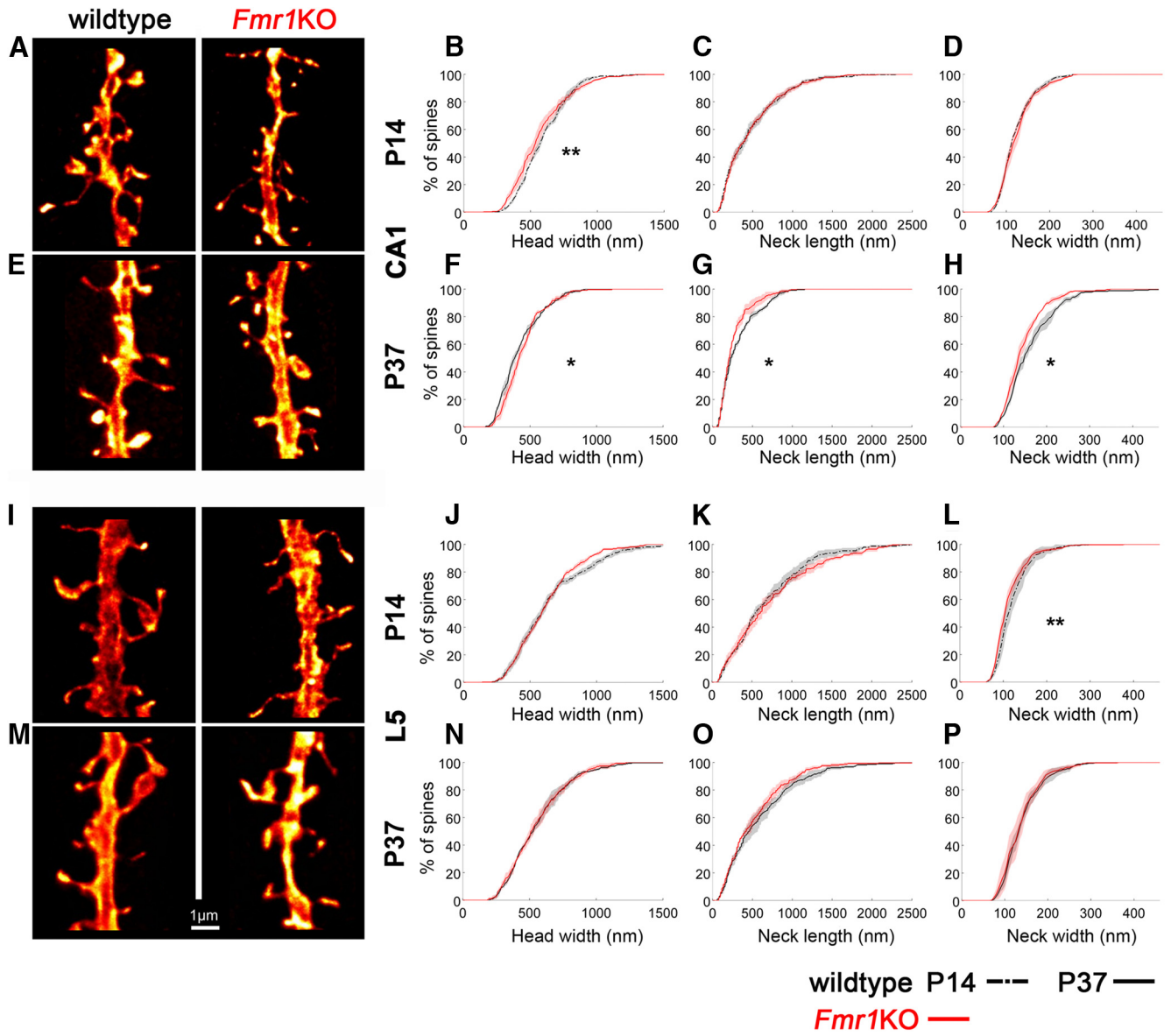

Figure 3. Loss of FMRP affects spine morphology at the nanoscale in an age and brain region-specific manner. ***A***, ***E***, ***I***, ***M***, Dendritic segments from CA1 and L5 pyramidal cells from wildtype and *Fmr1*KO mice at P14 (***A***, ***I***) and P37 (***E***, ***M***) show age and brain region-specific spine morphology changes. ***B***, At P14, the cumulative frequency distributions of spine head widths in CA1 significantly differ between genotypes (Kolmogorov–Smirnov test: $p = 0.007$). ***C***, ***D***, No differences are observed for spine neck lengths (***C***) and widths (***D***). ***F–H***, At P37, the distribution profiles of spine head widths (***F***), neck lengths (***G***), and neck widths (***H***) in CA1 are all significantly different between genotypes (Kolmogorov–Smirnov test: for head width, $p = 0.03$; for neck length, $p = 0.02$; for neck width, $p = 0.04$). ***J–P***, For L5 cells, only the distribution profile of spine neck widths is significantly different at P14 (***L***; Kolmogorov–Smirnov test: *P* value = 0.004) between genotypes (***J–P***). Here, whether the *P* value is considered significant or not is corrected for using the false discovery rate method, which controls false positives during multiple comparisons. Shaded areas show the interanimal variability. Scale bar, 1 μm. *$p < 0.05$; **$p < 0.01$.

was measured from the origin of spine at the dendritic shaft to the base of spine head. Head width was defined as the widest diameter of the head perpendicular to the spine length. Neck width was defined as the narrowest neck width, and was the full width half maximum of the Lorentzian curve fitted to this line profile. Protrusions that appeared to be "filopodia" (<5% of total protrusions) or "stubby," where a distinct neck region could not be discerned (<13% of total protrusions), were not included in the neck analysis. For wildtype mice at P14, for CA1 366 spines and for L5 266 spines from 4 animals were analyzed. At P37, for CA1 258 spines and for L5 293 spines from 3 animals were analyzed. For *Fmr1*KO mice at P14, for CA1 400 spines and for L5 376 spines analyzed from 5 and 6 animals, respectively. At P37, for CA1 237 spines and for L5 264 spines analyzed from 3 animals. For all, spines on 3–5 dendrites per animal were analyzed where each dendrite was acquired from a different cell.

Statistical analysis. The distributions of spine morphological parameters were compared using the nonparametric Kolmogorov–Smirnov test with the false discovery rate method to correct for multiple comparisons. For multiple comparisons between ages and brain regions with genotype, a two-way ANOVA with *post hoc* Bonferroni's multiple comparisons was used. Covariance between spine morphology parameters was tested using correlation and linear regression analyses, yielding the coefficient of determination (R^2).

Results

Spine heads become smaller and necks become shorter and wider with age

To elucidate brain region-dependent changes during normal development, we imaged spines on apical dendrites from CA1 and

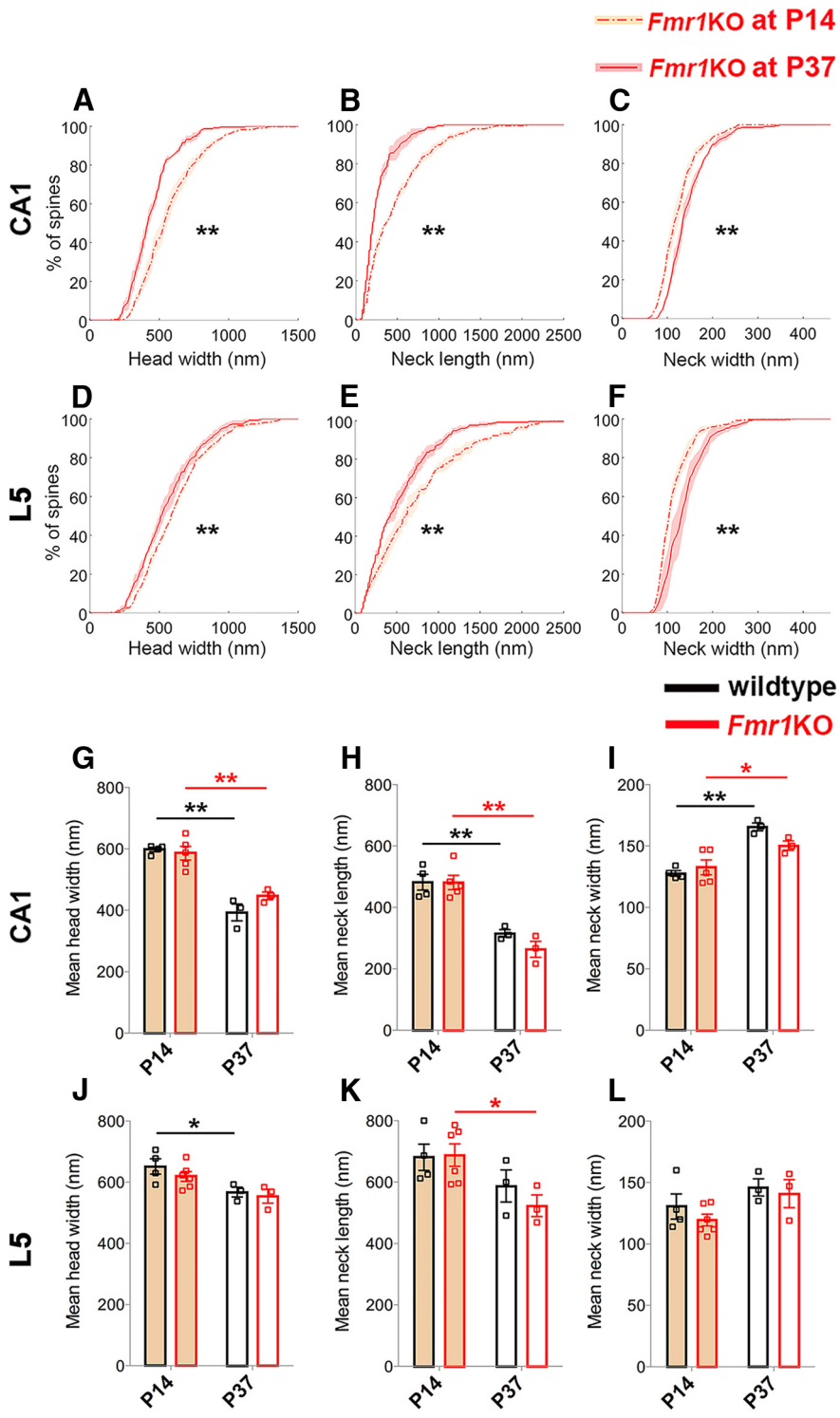

Figure 4. The developmental trajectory of spine morphogenesis is essentially maintained in the absence of FMRP. ***A–F***, For both CA1 and L5, the cumulative frequency distributions of spine head width (***A***, ***D***), neck length (***B***, ***E***), and neck width (***C***, ***F***) all significantly differ between P14 and P37 in *Fmr1*KO mice (Kolmogorov–Smirnov test: in CA1, for all $p < 0.0001$; in L5, for head width, $p = 0.009$; for neck length, $p = 0.006$; for neck width, $p < 0.0001$). Here, whether the *P* value is considered significant or not is corrected for using the false discovery rate method, which controls false positives during multiple comparisons. Using two-way ANOVA with *post hoc* Bonferroni multiple comparisons, mean differences in these parameters also show that the *Fmr1*KO mice mimic the developmental changes that occur in wildtype mice. For both regions, there is only a significant age effect of the morphological parameters. ***G–I***, In CA1, for head width (***G***): $F_{(1,11)} = 73.39$, $p < 0.0001$; for neck length (***H***): $F_{(1,11)} = 61.06$, $p < 0.0001$; for neck width (***I***): $F_{(1,11)} = 32.62$, $p = 0.0001$. ***J–L***, In L5, for head width (***J***): $F_{(1,12)} = 12.28$, $p = 0.004$; for neck length (***K***): $F_{(1,12)} = 8.64$, $p = 0.01$; and for neck width (***L***): $F_{(1,12)} = 5.03$, $p = 0.04$. Shaded areas around lines show interanimal variability. In bar graphs, data are represented as mean ± SEM, where n = number of animals. *$p < 0.05$; **$p < 0.01$.

L5 pyramidal cells (Fig. 1; Table 1). For both regions, cumulative frequency distributions show that there are more spines with smaller heads (Fig. 1*B*,*F*), and shorter and wider necks at P37 than at P14 (Fig. 1*C*,*D*,*G*,*H*). These developmental changes can be seen at the level of animal means and are more pronounced in CA1 than in L5 pyramidal cells (Fig. 1*I–K*). Moreover, spines on L5 pyramidal cells have a wider head and longer neck compared with spines on CA1 pyramidal cells at P37 (Fig. 1*I*,*J*).

Next, we examined whether there were any correlations between morphological parameters in our dataset. We found no strong correlations among any of the parameters examined in both brain regions and at both ages (Fig. 2), indicating that spine morphology covers a broad continuum of uncorrelated shapes and sizes; thus questioning the usefulness of simple categorization schemes commonly used in the literature.

Spine morphogenesis is largely intact in *Fmr1*KO mice, displaying only subtle deviations depending on age and brain region

We next tested the hypothesis that fragile X mental retardation protein (FMRP), the protein lost in FXS, regulates spine morphology in an age-dependent and region-dependent manner (Fig. 3; Table 1). In CA1 at P14 (Fig. 3*A–D*), the cumulative frequency distributions for *Fmr1*KO mice show fewer spines with wider heads (<800 nm) compared with wildtype mice, but no changes in neck lengths or widths between genotypes. In CA1 at P37 (Fig. 3*E–H*), *Fmr1*KO mice have more spines with large heads and shorter and narrower necks compared with wildtype mice. In contrast, the morphology of spines on L5 pyramidal cells is largely unaffected by the loss of FMRP (Fig. 3*I–P*). Only the distribution profiles of neck widths are significantly different at P14 with more spines having narrower necks in *Fmr1*KO mice (Fig. 3*L*), a phenotype that is not seen at P37 (Fig. 3*P*). While there are subtle changes in spine morphology associated with the loss of FMRP that depend on age and brain region, the overall developmental trajectory of spine morphogenesis is maintained (Fig. 4). No differences are observed in spine densities (mean spine density/10 μm ± SEM in wildtype vs *Fmr1*KO mice: at P14 in CA1, 12.23 ± 1.54 vs 10.98 ± 1.35; in L5, 10.99 ± 1.02 vs

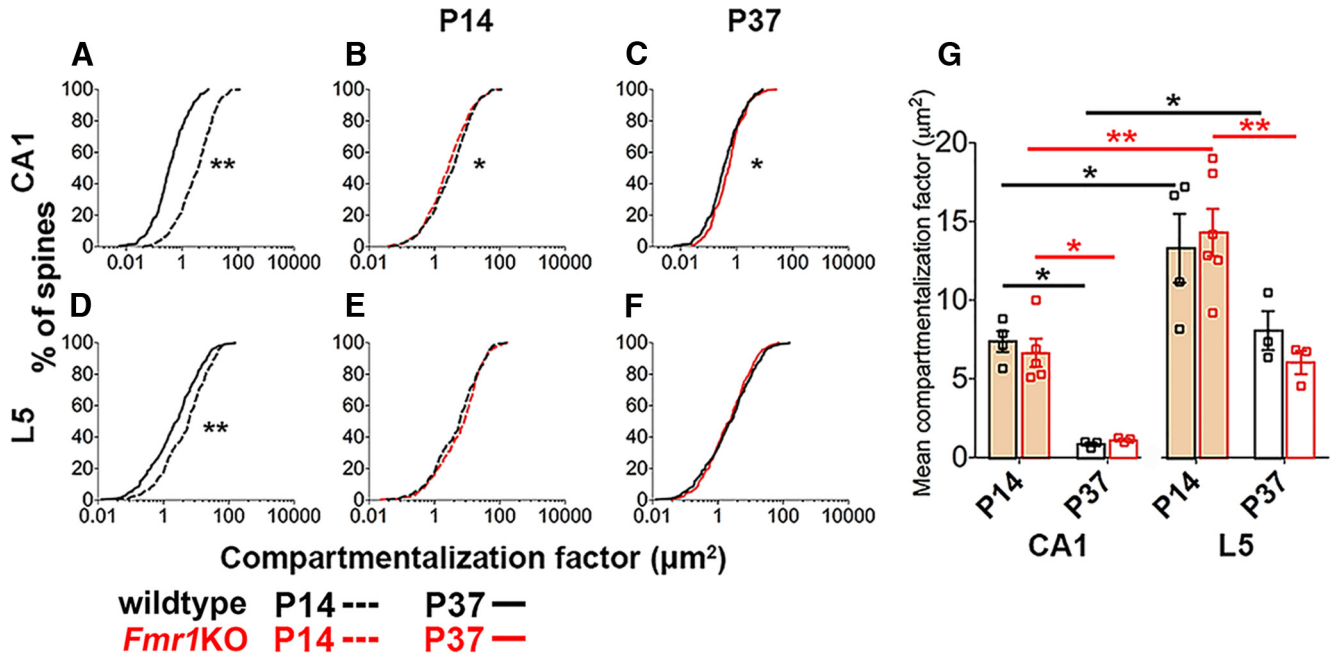

Figure 5. The developmental spine morphology changes predict decreased biochemical compartmentalization with age, while loss of FMRP subtly influences this in an age and brain region-specific manner. ***A***, ***D***, During normal development, cumulative frequency distributions of compartmentalization factor significantly differ between ages for spines on both CA1 (***A***) and L5 (***D***) pyramidal cells (Kolmogorov–Smirnov test: $p < 0.0001$). The compartmentalization factor decreases with age, thus predicting decreased biochemical compartmentalization. ***B***, ***C***, In CA1, there are age-specific changes to the distribution of compartmentalization factor with loss of FMRP (Kolmogorov–Smirnov test: P14, $p = 0.04$; P37, $p = 0.05$) predicting decreased biochemical compartmentalization at P14 (***B***), but increased biochemical compartmentalization at P37 (***C***). ***E***, ***F***, Conversely, loss of FMRP does not affect the distributions of compartmentalization factor for spines on L5 pyramidal cells. Here, whether the *P* value is considered significant or not is corrected for using the false discovery rate method, which controls false positives during multiple comparisons. ***G***, Using two-way ANOVA with *post hoc* Bonferroni multiple comparisons, mean differences in compartmentalization factor show age and brain region-specific differences in the magnitude of the effects during development, but not between the genotypes. For wildtype mice, age effect: $F_{(1,10)} = 16.37$, $p = 0.002$; region effect: $F_{(1,10)} = 20.55$, $p = 0.001$ with no significant interaction. For *Fmr1*KO mice, age effect: $F_{(1,13)} = 27.40$, $p = 0.0002$; region effect: $F_{(1,13)} = 22.76$, $p = 0.0004$ with no significant interaction. In bar graphs, data are represented as mean ± SEM, where n = number of animals. $^*p < 0.05$; $^{**}p < 0.01$.

10.84 ± 0.38; at P37 in CA1, 10.94 ± 1.43 vs 12.55 ± 1.46; in L5, 13.26 ± 0.80 vs 13.48 ± 0.88).

Synapse compartmentalization decreases with age in normal and *Fmr1*KO mice

We explored how changes in spine morphology might influence synapse compartmentalization, i.e., the ability of spines to process electrochemical signals in isolation from the parent dendrite, which depends strongly on spine morphology (Tonnesen et al., 2014). To predict the impact of developmental changes in spine morphology on diffusional coupling, we calculated a morphological "compartmentalization factor," defined as VL/A, where V is the head volume, L is the neck length, and A is the cross-sectional area of the spine neck. VL/A corresponds to the time constant τ of molecular equilibration after a step change in concentration for a simple compartmental model of diffusion ($\tau = VL/DA$, where D is diffusion coefficient of a given molecule, which was kept constant here; Alvarez and Sabatini, 2007).

Our data indicate that the compartmentalization factor substantially decreases during normal development both in CA1 and L5 pyramidal cells (Fig. 5*A*,*D*). The compartmentalization factor is smaller at P14 in CA1 compared with L5 spines and also decreases more in CA1 during development (Fig. 5*G*), indicating that synapse compartmentalization is developmentally regulated in a brain region-dependent manner.

Next, we compared the compartmentalization factor between *Fmr1*KO and wildtype mice in both brain regions and at both ages. At P14, spines on CA1 pyramidal cells have slightly smaller compartmentalization factors in *Fmr1*KO mice than in wildtype mice (Fig. 5*B*), corresponding to their smaller head sizes. However, at P37 this difference is reversed as spines in *Fmr1*KO mice have slightly larger compartmentalization factors, matching their larger heads and narrower necks, compared with wildtype mice (Fig. 5*C*). By contrast, no significant genotypic differences are seen for the compartmentalization factor in L5 at either developmental time point (Fig. 5*E*–*G*).

Together, the changes in compartmentalization factor during normal development are substantial, whereas the effects associated with the loss of FMRP are very subtle in CA1 and undetectable in L5.

Discussion

We analyzed spine morphogenesis in normal mice and in a mouse model of FXS using STED microscopy, yielding precise and quantitative measurements of key spine morphological parameters. Our findings challenge the current dogma of normal spine development and how it is affected in FXS. Notably, we observed marked developmental changes in spine morphology indicative of a substantial drop in synapse compartmentalization with age. Surprisingly, in *Fmr1*KO mice this developmental trajectory is largely maintained, with only subtle age-dependent and brain region-dependent deviations.

Normal development of spine morphology

Spine morphology is intimately related to synapse function, as spine head size correlates with synaptic strength (Nusser et al., 1998; Matsuzaki et al., 2001) and undergoes changes during synaptic plasticity (Lang et al., 2004; Matsuzaki et al., 2004; Nägerl et

al., 2004; Oh et al., 2013). In addition, recent studies show that spine necks exert a strong influence on electrochemical compartmentalization of dendritic spines (Harnett et al., 2012; Tonnesen et al., 2014).

Our STED analysis shows that spines become smaller and spine necks grow wider during the period of development when spine turnover decreases and synaptic circuits become established. These changes suggest a more complicated developmental program for spinogenesis than the commonly held belief that larger, more distinct ("mushroom-like") spines develop from thin and amorphously shaped ("filopodial") structures in parallel to their functional maturation.

These marked structural changes in dendritic spine morphology are indicative of a substantial increase with age in electrochemical coupling between spines and dendrites. The relative autonomy of spines in younger animals might be necessary for discriminating synapses based on varying synaptic efficacies, facilitating competitive mechanisms that refine synaptic connectivity during development. By contrast, once synapse selection has occurred, more permissive spine–dendrite crosstalk might be advantageous to allow for more cooperative and complex interactions between neighboring synapses, possibly boosting the computational power of dendrites in the mature brain. Our finding that spines become smaller and lose some of their neck definition during development is consistent with previous electron microscopy work (Harris et al., 1992), which reported more "thin" spines (i.e., spines with smaller heads) with smaller postsynaptic densities and shorter necks in the adult (P40–P70) compared with young (P14) rat hippocampal brain tissue.

Spines are traditionally classified into discrete morphological categories based on their appearance in electron micrographs (Peters and Kaiserman-Abramof, 1970; Harris et al., 1992). However, it has become clear that simple classification schemes (e.g., thin, stubby, mushroom, or filopodial spines) widely used in the literature do not accurately reflect the broad continuum of spine shapes and sizes that have been quantitatively described in more recent work based on electron (Benavides-Piccione et al., 2002; Arellano et al., 2007) or STED microscopy in live brain tissue sections (Tonnesen et al., 2014). In agreement with these previous studies, we did not find any strong correlations among the morphological parameters, raising questions about the common practice of assigning spines to distinct morphological categories.

Spine phenotype in the absence of FMRP

Our second main finding is that the developmental trajectory of spine morphology is largely intact in *Fmr1*KO mice, with only subtle changes that depend on age and brain region. In fact, at P14 in CA1, the morphological changes are indicative of a slightly reduced state of synapse compartmentalization, while at P37 the morphological effects on compartmentalization are counterbalanced as spines have larger heads, but also narrower and shorter necks. Nevertheless, the spine morphological changes at P37 suggest a subtle functional immaturity of spines in *Fmr1*KO mice as the changes predict a synapse compartmentalization slightly higher than that in wildtype mice.

Given that the changes in spine morphology in *Fmr1*KO mice are relatively subtle, it is unlikely that they provide a satisfactory explanation for the functional deficits associated with FXS. However, as dendritic integration across thousands of synapses is complex and highly nonlinear, it is possible that even subtle changes in synaptic compartmentalization could affect neural circuit function. Moreover, we cannot exclude the possibility that the loss of FMRP leads to defects in the specificity of synaptic connections or affects dynamic aspects of the structure–function relationship of synapses, such as activity-dependent structural plasticity. In support of this possibility, studies have reported a change in spine turnover in *Fmr1*KO mice (Cruz-Martin, 2010; Pan et al., 2010).

Our data clearly contrast with the classical view of an increased proportion of long, thin, and tortuous spines in FXS as first described by Rudelli et al. (1985). While some studies do recapitulate this spine phenotype, others do not (for review, see He and Portera-Cailliau, 2013). In particular our findings seem at odds with several studies that found an increase in spine length in *Fmr1*KO mice (Comery et al., 1997; Nimchinsky et al., 2001; Galvez and Greenough, 2005). Direct comparison between studies is difficult due to differences in methodology, age (Galvez and Greenough, 2005), brain region (Comery et al., 1997), and statistical analyses (Nimchinsky et al., 2001). Nonetheless, our findings and those of other laboratories, highlight that the effects of FMRP loss on spine morphology cannot be generalized between ages, brain regions or cell types. For example, while Galvez and Greenough (2005) found an increase in spine length for L5 pyramidal cells at P73–P76, no difference was observed at P25. Similarly, no differences in spine length were seen at 1 month (Pan et al., 2010) or at P21 (Nimchinsky et al., 2001). That said, in direct contrast to our findings, Nimchinsky et al. (2001) found an increase in spine length at P14. This difference between the two studies could be explained by the fact that Nimchinsky et al. (2001) sampled spines on both secondary apical and primary and tertiary basal segments, while we sample from secondary apical obliques located on the L4/5 boundary and upper L5. Finally, similar to previous studies that found no differences in spine density during the second and third postnatal weeks (Nimchinsky et al., 2001; Cruz-Martín et al., 2010), we also found no differences in spine density between wildtype and *Fmr1*KO mice at P14 or P37.

Spine dysgenesis is often thought to be a core neuropathology associated with NDDs. In an increasing number of cases, the rescue of spine morphology in animals by a given pharmacological compound is being used as a criterion for clinical trials. Our findings demonstrate that the morphological pathology associated with dendritic spines of cells lacking FMRP is more subtle than current dogma suggests. Furthermore, they strongly caution against generalizing between brain regions and developmental stages. Finally, they highlight the need for super-resolution imaging to address the functional consequences of altered spine morphology to better understand the neuropathology associated with models of NDDs.

References

Alvarez VA, Sabatini BL (2007) Anatomical and physiological plasticity of dendritic spines. Annu Rev Neurosci 30:79–97. CrossRef Medline

Arellano JI, Benavides-Piccione R, Defelipe J, Yuste R (2007) Ultrastructure of dendritic spines: correlation between synaptic and spine morphologies. Front Neurosci 1:131–143. CrossRef Medline

Benavides-Piccione R, Ballesteros-Yáñez I, DeFelipe J, Yuste R (2002) Cortical area and species differences in dendritic spine morphology. J Neurocytol 31:337–346. CrossRef Medline

Bethge P, Chéreau R, Avignone E, Marsicano G, Nägerl UV (2013) Two-photon excitation STED microscopy in two colors in acute brain slices. Biophys J 104:778–785. CrossRef Medline

Brose N, O'Connor V, Skehel P (2010) Synaptopathy: dysfunction of synaptic function? Biochem Soc Trans 38:443–444. CrossRef Medline

Comery TA, Harris JB, Willems PJ, Oostra BA, Irwin SA, Weiler IJ, Greenough WT (1997) Abnormal dendritic spines in fragile X knockout

mice: maturation and pruning deficits. Proc Natl Acad Sci U S A 94:5401–5404. CrossRef Medline

Cruz-Martín A, Crespo M, Portera-Cailliau C (2010) Delayed stabilization of dendritic spines in fragile X mice. J Neurosci 30:7793–7803. CrossRef Medline

Feng G, Mellor RH, Bernstein M, Keller-Peck C, Nguyen QT, Wallace M, Nerbonne JM, Lichtman JW, Sanes JR (2000) Imaging neuronal subsets in transgenic mice expressing multiple spectral variants of GFP. Neuron 28:41–51. CrossRef Medline

Galvez R, Greenough WT (2005) Sequence of abnormal dendritic spine development in primary somatosensory cortex of a mouse model of the fragile X mental retardation syndrome. Am J Med Genet A 135:155–160. Medline

Harnett MT, Makara JK, Spruston N, Kath WL, Magee JC (2012) Synaptic amplification by dendritic spines enhances input cooperativity. Nature 491:599–602. CrossRef Medline

Harris KM, Jensen FE, Tsao B (1992) Three-dimensional structure of dendritic spines and synapses in rat hippocampus (CA1) at postnatal day 15 and adult ages: implications for the maturation of synaptic physiology and long-term potentiation. J Neurosci 12:2685–2705. Medline

He CX, Portera-Cailliau C (2013) The trouble with spines in fragile X syndrome: density, maturity and plasticity. Neuroscience 251:120–128. CrossRef Medline

Hell SW, Wichmann J (1994) Breaking the diffraction resolution limit by stimulated emission: stimulated-emission-depletion fluorescence microscopy. Opt Lett 19:780–782. Medline

Holtmaat AJ, Trachtenberg JT, Wilbrecht L, Shepherd GM, Zhang X, Knott GW, Svoboda K (2005) Transient and persistent dendritic spines in the neocortex in vivo. Neuron 45:279–291. CrossRef Medline

Lang C, Barco A, Zablow L, Kandel ER, Siegelbaum SA, Zakharenko SS (2004) Transient expansion of synaptically connected dendritic spines upon induction of hippocampal long-term potentiation. Proc Natl Acad Sci U S A 101:16665–16670. CrossRef Medline

Li JY, Plomann M, Brundin P (2003) Huntington's disease: a synaptopathy? Trends Mol Med 9:414–420. CrossRef Medline

Matsuzaki M, Ellis-Davies GC, Nemoto T, Miyashita Y, Iino M, Kasai H (2001) Dendritic spine geometry is critical for AMPA receptor expression in hippocampal CA1 pyramidal neurons. Nat Neurosci 4:1086–1092. CrossRef Medline

Matsuzaki M, Honkura N, Ellis-Davies GC, Kasai H (2004) Structural basis of long-term potentiation in single dendritic spines. Nature 429:761–766. CrossRef Medline

Mientjes EJ, Nieuwenhuizen I, Kirkpatrick L, Zu T, Hoogeveen-Westerveld M, Severijnen L, Rifé M, Willemsen R, Nelson DL, Oostra BA (2006) The generation of a conditional Fmr1 knock out mouse model to study Fmrp function in vivo. Neurobiol Dis 21:549–555. CrossRef Medline

Nägerl UV, Eberhorn N, Cambridge SB, Bonhoeffer T (2004) Bidirectional activity-dependent morphological plasticity in hippocampal neurons. Neuron 44:759–767. CrossRef Medline

Nägerl UV, Willig KI, Hein B, Hell SW, Bonhoeffer T (2008) Live-cell imaging of dendritic spines by STED microscopy. Proc Natl Acad Sci U S A 105:18982–18987. CrossRef Medline

Nimchinsky EA, Oberlander AM, Svoboda K (2001) Abnormal development of dendritic spines in *FMR1* knock-out mice. J Neurosci 21:5139–5146. Medline

Nusser Z, Lujan R, Laube G, Roberts JD, Molnar E, Somogyi P (1998) Cell type and pathway dependence of synaptic AMPA receptor number and variability in the hippocampus. Neuron 21:545–559. CrossRef Medline

Oh WC, Hill TC, Zito K (2013) Synapse-specific and size-dependent mechanisms of spine structural plasticity accompanying synaptic weakening. Proc Natl Acad Sci U S A 110:E305–E312. CrossRef Medline

Pan F, Aldridge GM, Greenough WT, Gan WB (2010) Dendritic spine instability and insensitivity to modulation by sensory experience in a mouse model of fragile X syndrome. Proc Natl Acad Sci U S A 107:17768–17773. CrossRef Medline

Penzes P, Cahill ME, Jones KA, VanLeeuwen JE, Woolfrey KM (2011) Dendritic spine pathology in neuropsychiatric disorders. Nat Neurosci 14:285–293. CrossRef Medline

Peters A, Kaiserman-Abramof IR (1970) The small pyramidal neuron of the rat cerebral cortex. The perikaryon, dendrites and spines. Am J Anat 127:321–355. CrossRef Medline

Porrero C, Rubio-Garrido P, Avendaño C, Clascá F (2010) Mapping of fluorescent protein-expressing neurons and axon pathways in adult and developing Thy1-eYFP-H transgenic mice. Brain Res 1345:59–72. CrossRef Medline

Rudelli RD, Brown WT, Wisniewski K, Jenkins EC, Laure-Kamionowska M, Connell F, Wisniewski HM (1985) Adult fragile X syndrome. Clinico-neuropathologic findings. Acta Neuropathol 67:289–295. CrossRef Medline

Tonnesen J, Katona G, Rozsa B, Nägerl UV (2014) Spine neck plasticity regulates synapse compartmentalization. Nat Neurosci. Advance online publication. Rereieved April 3, 2014. doi:10.1038/nn.3682. CrossRef Medline

Yuste R (2011) Dendritic spines and distributed circuits. Neuron 71:772–781. CrossRef Medline

Yuste R, Bonhoeffer T (2004) Genesis of dendritic spines: insights from ultrastructural and imaging studies. Nat Rev Neurosci 5:24–34. CrossRef Medline